PhD Second-Year Checkpoint

Summary Report

Full Name	Bruno Rodrigues Pacheco e Murta
Institution	Universidade do Minho
Doctoral Programme	MAP-fis
Title of Dissertation	Quantum Many-Body Ground States via Digital Quantum Simulation
Supervisor	Prof. Joaquín Fernández-Rossier (INL)
Co-Supervisor	Prof. Nuno M. R. Peres (U. Minho)

Executive Summary

The overarching goal of the research project undertaken by Bruno Murta during his doctoral studies is to explore methods to prepare on a digital quantum computer ground states of quantum condensed matter systems, notably those comprising strongly-correlated electrons, on the one hand, and frustrated spins, on the other. Concretely, Mr. Murta's contributions are framed within the context of the development of physically-motivated trial states that can serve as a good first approximation of the exact ground states of quantum many-body systems.

To this end, over the past year, corresponding to the second of his doctoral studies, Mr. Murta has devised quantum computing schemes to prepare two reference quantum many-body states in condensed matter physics: the Gutzwiller wave function [1] and the Valence Bond States [2]. In both cases, the challenge lies in the implementation of a non-unitary operator — the Gutzwiller operator and the symmetrization operator, respectively — in terms of quantum gates, which are inherently unitary. This difficulty is overcome by embedding these non-unitary operations in a larger unitary one through the addition of ancillary qubits subject to measurement, the outcome of which is post-processed. Given the probabilistic nature of the resulting methods, a strategy to mitigate the repetition overhead was developed for the Valence Bond States, and alternative approaches to apply the Gutzwiller wave function to digital quantum simulation were identified, as discussed in the accompanying document that covers the updated PhD work plan.

The results of this work have been disseminated in different forms. Regarding the Gutzwiller wave function project, a Letter was published in *Physical Review B* [3], and two oral contributions at conferences were accepted, one already delivered at the 2021 APS March Meeting and the other to be given this month at the 3$^{\text{rd}}$ Condensed Matter Physics National Conference. As for the Valence Bond States project, an article is currently in preparation.

Besides the aforementioned research accomplishments, Mr. Murta has also developed valuable skills in quantum computing (e.g., implementation of fixed-point quantum amplitude amplification [4], preparation of mean-field states [5]) and consolidated his background in quantum condensed matter physics (e.g., exploration of tensor network methods [6, 7] as part of a study group, delivery of tutorial on Kitaev honeycomb model [8] at internal group meetings).

The remainder of this report is structured as follows. The next section introduces the overarching motivation of this PhD project, presenting it in the broader context of digital quantum simulation as a novel paradigm to study quantum many-body phenomena and introducing some key concepts and methods of the field. The following section provides a brief but self-contained outline of the research completed over the last year. It comprises two subsections, one devoted to the Gutzwiller wave function and the other to Valence Bond States. The last section details additional activities carried out in this period, namely learning processes and the dissemination of research results.

Introduction: Motivation of PhD Project

Quantum many-body phenomena are ubiquitous in condensed matter physics. However, their understanding has been hampered by the difficulty in performing large-scale numerical simulations, which are crucial to probe the emergent nature of these phenomena [9]. Indeed, Density-Functional Theory [10, 11] can quantitatively account for the low-energy properties of weakly interacting materials with approximate functionals based on the Local Density Approximation [12], but not in the presence of strong electron-electron interactions. Quantum Monte Carlo [13] methods, in turn, face the infamous sign problem [14] for fermions or half-integer spins in non-bipartite lattices.

A more accurate description of correlated fermions or frustrated spins could, in principle, be achieved by considering the wave function explicitly, but the exponential scaling of the Hilbert space with the system size ultimately exceeds the memory capacity of conventional hardware, even when ingenious tensor network methods [6] are used, at least beyond one spatial dimension. This is, however, not the case in quantum hardware, thanks to the principle of superposition and the natural encoding of entanglement [15]. Quantum computers are therefore a natural platform to simulate quantum many-body systems [16].

Several quantum algorithms to determine the ground state of a given Hamiltonian $\mathcal{H}$ have been proposed, the most prominent examples being quantum phase estimation [17] (QPE) for large-scale fault-tolerant quantum hardware and the variational quantum eigensolver (VQE) [18] for noisy intermediate-scale quantum computers. In spite of the development of these algorithms, it is well established [19] that the problem of finding the ground state of Hamiltonians involving only local interactions is, in general, QMA-complete[1], which means that even a large-scale fault-tolerant quantum computer would struggle to solve such problems by brute force. This complexity can be traced back to the preparation of an initial state that is sufficiently close to the exact ground state.

Indeed, the scaling of QPE is polynomial with respect to the inverse of the overlap between the initial state and the exact ground state [20], so the initial state preparation routine should lead to a polynomially decreasing overlap as the system size increases for the overall algorithm to be efficient [21]. Nevertheless, conventional choices of initial states, such as noninteracting or mean-field ground states, produce an exponentially vanishing probability of collapsing into the ground state due to the orthogonality catastrophe [22], thus demanding an exponential number of repetitions of QPE to achieve success. This overlap can, in principle, be enhanced via adiabatic evolution [23], but its viability depends on the gap between the ground and first excited states throughout the adiabatic path, which is generally unknown and may even close.

Contrary to QPE, VQE is a heuristic method, in the sense that there is no guarantee that, for a given input state, the exact ground state will be attained. In fact, the challenge in VQE is not just preparing a good initial state, but also formulating a parameterized ansatz such that its manifold includes a path connecting the initial state to the exact ground state without incurring in an exponential number of parameters. An exceedingly large number of parameters has three negative implications: first, the greater difficulty of the classical optimization problem; second, the increase of the circuit depth beyond what can be faithfully executed with near-term quantum hardware; third, the flattening of the parameter landscape, whereby its distinctive features are localized in very small regions — the so-called *barren plateau* problem [24].

Whether one opts for QPE or VQE, in order to use quantum computers to solve quantum many-body problems that defy state-of-the-art numerical methods on conventional hardware, it is imperative to exploit physical insights about the system to construct sufficiently close initial approximations of the exact ground state, as well as highly expressive but lean ansätze for the particular case of hybrid variational methods such as VQE. This is the overarching goal of this PhD project.

[1] QMA, short for *Quantum Merlin-Arthur*, is the quantum analog of the complexity class NP.

Completed Research: Brief Outline

Gutzwiller Wave Function

In light of the importance of trial states in digital quantum simulation algorithms, Mr. Murta and his supervisor, Prof. Joaquín Fernández-Rossier, have devised a method [3] to prepare on quantum hardware the Gutzwiller Wave Function [1] (GWF), which can be defined as

$$|\psi_G\rangle = \prod_{i=1}^{N} (\mathbb{1} - g\hat{n}_{i,\uparrow}\hat{n}_{i,\downarrow}) \, |\psi_0\rangle \, , \tag{1}$$

where $g \in [0, 1]$ is a free parameter, N is the number of lattice sites, $|\psi_0\rangle$ is the noninteracting ground state, and $\hat{n}_{i,\alpha} \equiv \hat{a}^{\dagger}_{i,\alpha}\hat{a}_{i,\alpha}$ is the number operator acting on site i for electrons of spin $\alpha = \uparrow, \downarrow$, with $\hat{a}_{i,\alpha}$ the annihilation operator in second quantization. In words, the GWF is prepared by reducing the amplitude of the basis states of $|\psi_0\rangle$ with doubly-occupied sites. The degree of this reduction is set by g, the optimal value of which is found by minimizing the energy.

Despite its apparent simplicity, the GWF is a quantum many-body state that captures some correlations between the electrons. Indeed, the noninteracting ground state, $|\psi_0\rangle = \prod_{\alpha,\sigma} \hat{a}^{\dagger}_{\alpha,\sigma} |0\rangle$, is a Fock state in the eigenbasis $\{|\alpha\rangle\}$ of the tight-binding Hamiltonian. However, the Gutzwiller operator is applied in real space, so the operators $\{\hat{a}^{\dagger}_{\alpha,\sigma}\}$ have to be expressed as a linear combination of site operators $\{\hat{a}^{\dagger}_{i,\sigma}\}$, so that $|\psi_0\rangle$ appears as multi-determinant state: $|\psi_0\rangle = \prod_{\alpha,\sigma} (\sum_i \phi_\alpha(i)\hat{a}^{\dagger}_{i,\sigma}) \, |0\rangle$. As a result, the determination of expectation values of the GWF is a many-body problem that cannot be solved exactly except in one [25, 26] and infinite dimensions [27].

To motivate the use of the GWF as a starting point for quantum simulation algorithms, the overlap of this ansatz with the exact ground state of Fermi-Hubbard chains at half-filling with up to $N = 12$ sites was compared to those of two standard choices of initial states: the noninteracting and the self-consistent mean-field ground states. The results are presented in Fig. 1 in two forms: (a) fixing the chain length ($N = 12$) and varying the interaction strength U/t; (b) fixing the interaction strength ($U/t = 10$) and varying the chain length N. The decrease of the overlap between the GWF and the exact ground state is significantly slower, which makes it a far better starting point for QPE or VQE than the single-particle states, especially for large systems.

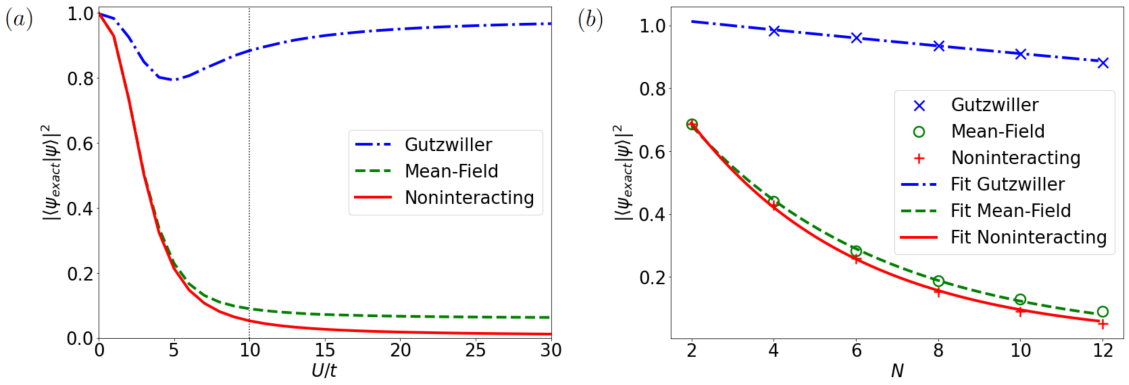

Figure 1: Comparison of Gutzwiller Wave Function to noninteracting and self-consistent mean-field ground states for Fermi-Hubbard chain at half-filling. (a) Fidelity of three reference states with respect to exact ground state for a chain of $N = 12$ sites against normalized Hubbard parameter U/t. (b) Same as (a), but now N is varied between 2 and 12 sites, while $U/t = 10$, as highlighted in (a) by the vertical dotted line. Numerical results were fitted to exponential decay $c_1 e^{-c_2 N}$.

The preparation of the GWF on a quantum computer entails the challenge of implementing the non-unitary Gutzwiller operator $\hat{P}_G^{(i)}(g) \equiv \mathbb{1} - g\hat{n}_{i,\uparrow}\hat{n}_{i,\downarrow}$ at every site $i = 1, 2, ..., N$ of the lattice (cf. eq. (1)). However, quantum gates are, by construction, unitary, since they ultimately correspond to time-evolution operators of closed quantum systems. To circumvent this problem, the Hilbert space on which each $\hat{P}_G^{(i)}(g)$ is applied is enlarged by adding one ancillary qubit. More concretely, the matrix representation of $\hat{P}_G^{(i)}(g)$ in the site basis is

$$\hat{P}_G^{(i)}(g) = \begin{pmatrix} 1 & 0 & 0 & 0 \\ 0 & 1 & 0 & 0 \\ 0 & 0 & 1 & 0 \\ 0 & 0 & 0 & 1-g \end{pmatrix}. \tag{2}$$

Applying the single-qubit gate

$$\mathcal{U}(g) = \begin{pmatrix} 1-g & -\sqrt{2g-g^2} \\ \sqrt{2g-g^2} & 1-g \end{pmatrix} \tag{3}$$

to the added ancillary qubit if and only if the two spin orbitals at site i are both occupied (i.e., the wave function at that site is in state $|\uparrow\downarrow\rangle$ or, equivalently, the two qubits that encode such site are in state $|11\rangle$) results in the three-qubit gate shown in Fig. 2(a). Noting that the top-left quadrant of this 8×8 matrix is precisely the 4×4 representation of $\hat{P}_G^{(i)}(g)$ (cf. eq. (2)), it follows that the Gutzwiller operator can be applied to site i of the noninteracting ground state $|\psi_0\rangle$ by preparing an ancillary qubit in state $|0\rangle$, executing the three-qubit gate $\mathrm{cc}\mathcal{U}(g)$ with such ancilla as the target qubit and the two qubits of site i as the control-qubits, and finally measuring the ancilla in the computational basis, retrieving only the outcomes that yield $|0\rangle$. This procedure can be extended to an arbitrary number of lattice sites, as described in Fig. 2(b).

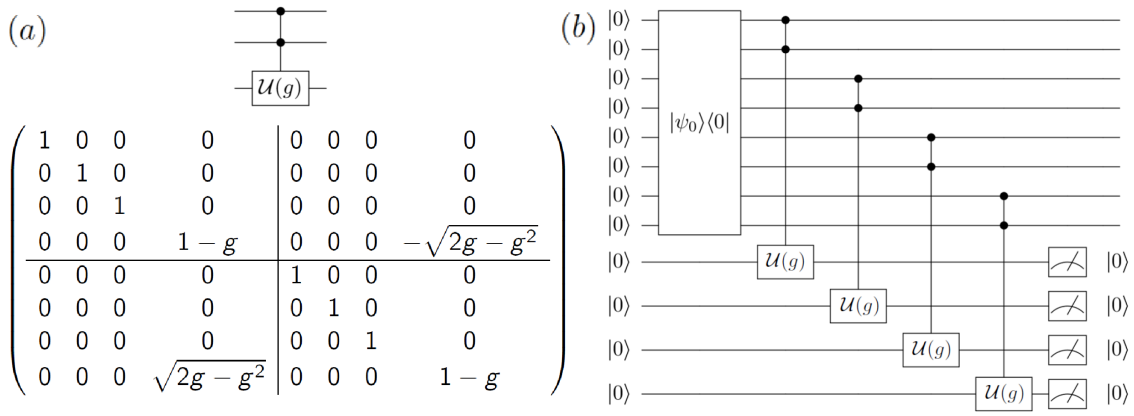

Figure 2: (a) Matrix representation of three-qubit gate $\mathrm{cc}\mathcal{U}(g)$ used to implement local Gutzwiller operator $\hat{P}_G^{(i)}(g) \equiv \mathbb{1} - g\hat{n}_{i,\uparrow}\hat{n}_{i,\downarrow}$ at every site. Top-left quadrant corresponds to 4×4 representation of $\hat{P}_G^{(i)}(g)$ in site basis. (b) Scheme of quantum circuit to prepare Gutzwiller wave function $|\psi_G\rangle = \prod_i \hat{P}_G^{(i)}(g)\,|\psi_0\rangle$, given subcircuit to prepare the noninteracting ground state $|\psi_0\rangle$ [5]. Scheme corresponds to a lattice with $N = 4$ sites.

Assuming the realistic case of linear qubit connectivity in the quantum hardware, the circuit depth of the preparation of the GWF scales as $\mathcal{O}(12N)$, which represents only a $\frac{3}{2}$-fold increase in the prefactor of the scaling corresponding to the preparation of the noninteracting ground state $|\psi_0\rangle$ (cf. Supplemental Material of [3] for detailed analysis). For sufficiently large lattices, the main bottleneck of this method is the repetition overhead due to its probabilistic nature — all ancillas have to be measured in site $|0\rangle$ to prepare the GWF. However, for lattice sizes that are beyond the reach of conventional numerical methods ($N \sim 30 - 40$), this overhead is still feasible [3].

Valence Bond States

Unlike the Gutzwiller wave function, the class of quantum many-body states covered in this section, the Valence Bond States (VBS), are the exact ground states of quantum spin models known as Affleck-Kennedy-Lieb-Tasaki (AKLT) models [2]. As a result, the purpose of preparing a VBS on digital quantum computers is not to probe the properties of the VBS itself — which can be studied analytically or, if required, using its exact tensor network representation [28] — but rather to use the VBS as the starting point to determine other eigenstates of its parent Hamiltonian or of nearby non-integrable ones, particularly using hybrid variational algorithms such as VQE in near-term quantum hardware.

The overarching motivation of this project is the prospect of employing the ground state of a naturally-occurring Hamiltonian such as the spin-$\frac{3}{2}$ AKLT model on the honeycomb lattice [29, 30], or possibly a nearby but non-integrable model, as a resource state for measurement-based quantum computation [31, 32, 33]. Information about the size of the spectral gap and the nature of the low-lying excited states of this parent Hamiltonian could provide valuable assistance in the experimental realization of such a robust resource state. However, computing these properties using conventional numerical methods is a formidable challenge, as demonstrated by the recent proof of the nonzero gap of the spin-$\frac{3}{2}$ AKLT model [34, 35]. The challenge is certainly even more daunting away from the integrable point, where experimental systems are likely to be found [36].

In general, a spin-S VBS can be prepared in any lattice with coordination number $2S$ by associating $2S$ spins-$\frac{1}{2}$ with each site and performing the following two steps (cf. Fig. 3 for a schematic description for the particular case $S = 1$ in one dimension): first, a valence bond $\frac{1}{\sqrt{2}}(|\uparrow\downarrow\rangle - |\downarrow\uparrow\rangle)$ is created along every nearest-neighbor link so that every spin-$\frac{1}{2}$ is involved in one; second, the $2S$ spins-$\frac{1}{2}$ are symmetrized at every site to yield the expected local spin-S.

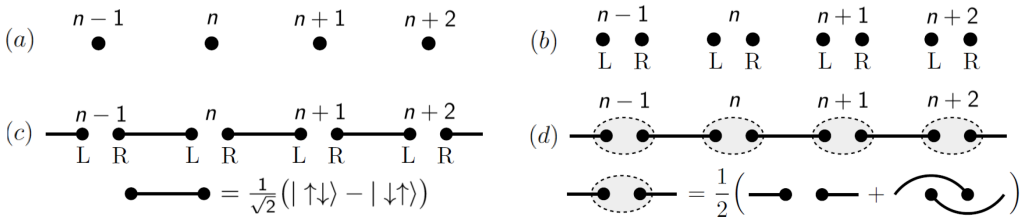

Figure 3: Schematic description of construction of spin-1 Valence Bond States in one dimension. (a) One-dimensional lattice with spin-1 at each site. (b) Each spin-1 is encoded in terms of 2 spins-$\frac{1}{2}$. (c) Each pair of spins-$\frac{1}{2}$ from neighboring sites forms a valence bond. (d) Two spins-$\frac{1}{2}$ at each site are symmetrized to generate the local spin-1. Figure retrieved from [28].

The AKLT models are constructed in such a way that the VBS is their ground state [2]. For concreteness, let us consider the spin-1 AKLT model in one dimension. Originally, the total spin of any pair of neighboring spins-1, $\vec{S}^{n,n+1}_{\text{total}} = \vec{S}_n + \vec{S}_{n+1}$, can take the values $1 \oplus 1 = 0, 1, 2$, where $\oplus$ denotes angular momentum addition. To dispose of $S^{n,n+1}_{\text{total}} = 2$, each local spin-1 is decomposed into two spins-$\frac{1}{2}$, so that a valence bond $\frac{1}{\sqrt{2}}(|\uparrow\downarrow\rangle - |\downarrow\uparrow\rangle)$ can be created between the two adjacent spins-$\frac{1}{2}$ for each pair of neighboring sites. Since the valence bond is a (spin-0) singlet, now $S^{n,n+1}_{\text{total}}$ can only take values $\frac{1}{2} \oplus 0 \oplus \frac{1}{2} = 0, 1$. Hence, if we define the AKLT Hamiltonian as

$$\mathcal{H}^{S=1}_{\text{AKLT}} = 2 \sum_{n=1}^{N-1} \left(P^{S=2}_{n,n+1}(\vec{S}_n, \vec{S}_{n+1}) - \frac{1}{3} \right) = \sum_{n=1}^{N-1} \vec{S}_n \cdot \vec{S}_{n+1} + \frac{1}{3}(\vec{S}_n \cdot \vec{S}_{n+1})^2, \tag{4}$$

where $P^{S=2}_{n,n+1}$ is a local projector that maps neighboring spins-1 to the subspace of total spin $S^{n,n+1}_{\text{total}} = 2$, we realize that, ignoring the additive constant, any state with no contribution from

the spin-2 component of any two neighboring spins-1 must have zero energy, which is the ground state energy as projectors are positive semi-definite operators. As a result, the spin-1 VBS is the ground state of the AKLT model defined in eq. (4).

It is straightforward to generalize this construction to lattices with greater coordination numbers. For example, in any lattice $\mathcal{L}$ with coordination number 3 (e.g., honeycomb lattice), the spin-$\frac{3}{2}$ VBS is the ground state of the AKLT Hamiltonian [2]

$$\mathcal{H}_{\text{AKLT}}^{S=\frac{3}{2}} = \sum_{(n,n')\in\mathcal{L}} P_{n,n'}^{S=3}(\vec{S}_n, \vec{S}_{n'}) = \sum_{(n,n')\in\mathcal{L}} \Big(\frac{11}{192} + \frac{27}{160}\vec{S}_n\cdot\vec{S}_{n'} + \frac{29}{360}(\vec{S}_n\cdot\vec{S}_{n'})^2 + \frac{1}{90}(\vec{S}_n\cdot\vec{S}_{n'})^3\Big), \quad (5)$$

where (n, n') denotes a pair of nearest-neighboring sites and $P_{n,n'}^{S=3}$ projects the sum of spins-$\frac{3}{2}$ $\vec{S}_n$ and $\vec{S}_{n'}$ onto the subspace of total spin $S_{\text{total}}^{n,n'} = 3$.

The initialization of a VBS on quantum hardware follows the two steps described above. The first step can be straightforwardly implemented by applying the two-qubit subcircuit shown in Fig. 4(a) at each pair of qubits representing the two spins-$\frac{1}{2}$ along a lattice link $(n, n') \in \mathcal{L}$. All such subcircuits can be applied in parallel, thus resulting in a layer of depth 1 CNOT. As in the Gutzwiller wave function, the challenge lies in the second step, due to the non-unitarity of the local symmetrization operator $\mathcal{S}$. This issue can be addressed by adding an ancillary qubit at each site to perform an Hadamard test (cf. Fig. 4(b)) [37].

Even though $\mathcal{S}$ is not unitary, it is Hermitian, so $e^{-i\theta\mathcal{S}}$ is unitary for any $\theta \in \mathbb{R}$ and we can, in principle, find the corresponding quantum circuit. Let us now consider the application of the Hadamard test (cf. Fig. 4(b)) with $\mathcal{U} = e^{-i\theta\mathcal{S}}$. Labelling the input state on the main register as $|\psi\rangle$, the output of this circuit before the measurement of the ancilla qubit is

$$|0\rangle \otimes \left[\frac{\mathbb{1} + e^{-i\theta\mathcal{S}}}{2}\right]|\psi\rangle + |1\rangle \otimes \left[\frac{\mathbb{1} - e^{-i\theta\mathcal{S}}}{2}\right]|\psi\rangle\,. \quad (6)$$

Using the idempotence of $\mathcal{S}$, $e^{-i\theta\mathcal{S}} = \mathbb{1} - (1 - e^{-i\theta})\mathcal{S}$. Replacing in (6) and setting $\theta = \pi$ gives

$$|0\rangle \otimes (\mathbb{1} - \mathcal{S})\,|\psi\rangle + |1\rangle \otimes \mathcal{S}\,|\psi\rangle\,. \quad (7)$$

Hence, applying the Hadamard test with $\mathcal{U} = e^{-i\pi\mathcal{S}}$ to an input state $|\psi\rangle$ and retaining only the measurements of the ancilla that yield $|1\rangle$ results in the application of $\mathcal{S}$ to $|\psi\rangle$ at the site in question. The generalization to N lattice sites follows trivially, as shown in Fig. 4(c).

Because the successful local symmetrization of all N sites requires the measurement of all ancillas in state $|1\rangle$, the resulting method is probabilistic. Ignoring finite-size effects, the average number of trials required to achieve a successful outcome is $(1/p)^N$, where $p \in (0, 1)$ is the fraction of symmetric spin states selected by $\mathcal{S}$ at each site [37]. In other words, p is the ratio between the number of states corresponding to the desired local spin-S and the total number of states resulting from adding the $2S$ spins-$\frac{1}{2}$ at each site. For the sake of clarity, let us consider the $S = 1$ case: the addition of $2S = 2$ spins-$\frac{1}{2}$ gives $\frac{1}{2} \oplus \frac{1}{2} = 0, 1$, so we have $2 \times 1 + 1 = 3$ spin-1 states and $2 \times 0 + 1 = 1$ spin-0 state, yielding $p = \frac{3}{4}$. Following the same logic, for $S = \frac{3}{2}$ we have $p = \frac{1}{2}$.

In light of this exponential scaling of the repetition overhead, devising a method to reduce the number of trials could be decisive to achieve quantum advantage with near-term quantum hardware. Mr. Murta and Prof. Fernández-Rossier devised a strategy [37] that produces a quadratic reduction in the repetition overhead at the cost of a logarithmic depth overhead. This strategy exploits the local entanglement structure of the product state of valence bonds that serves as input to the second step of the preparation of VBS corresponding to the local symmetrization.

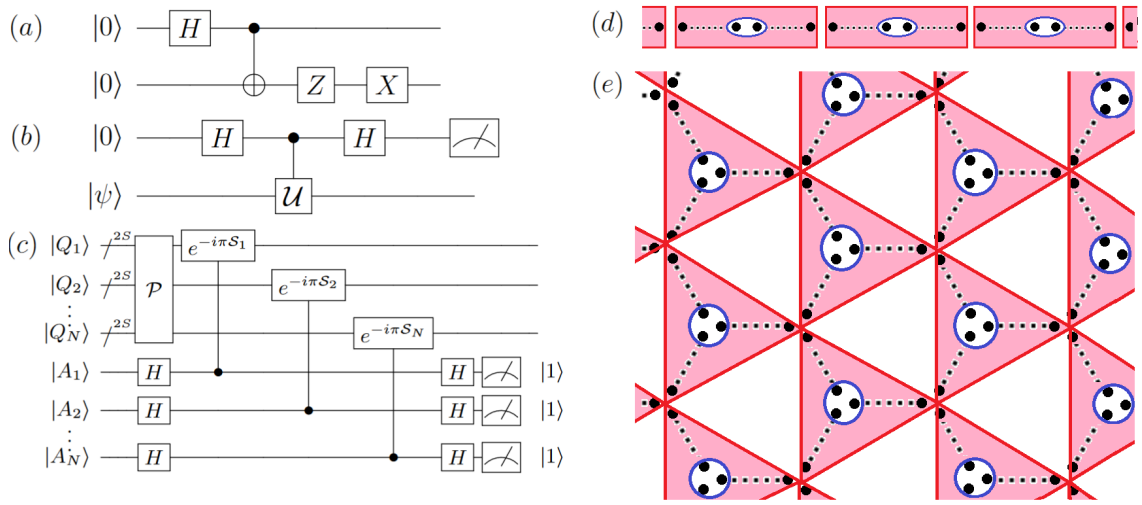

Figure 4: (a) Two-qubit subcircuit that prepares a single valence bond $1/\sqrt{2}(|\uparrow\downarrow\rangle - |\downarrow\uparrow\rangle)$. Full circuit $\mathcal{P}$ that executes first step of preparation of VBS, yielding $|\psi_{\text{pre-VBS}}\rangle \equiv \mathcal{P}\,|0\rangle^{\otimes 2NS}$, amounts to repetition of this subcircuit across all pairs of qubits representing lattice links. (b) Hadamard test for generic unitary operator $\mathcal{U}$. (c) Circuit that prepares spin-S Valence Bond State, $|\psi_{\text{VBS}}\rangle = \bigotimes_{n=1}^{N} \mathcal{S}_n\,|\psi_{\text{pre-VBS}}\rangle$, in N-site lattice if all N ancillas are measured in $|1\rangle$. All controlled-$e^{-i\pi\mathcal{S}_n}$ can be executed in parallel. (d,e) Scheme of product state of valence bonds, $|\psi_{\text{pre-VBS}}\rangle$, in one-dimensional lattice (d) and honeycomb lattice (e) to support explanation of repetition overhead mitigation scheme. Dashed black lines represent valence bonds and black dots denote qubits. 4-qubit islands within filled rectangles (d) and 6-qubit islands within filled triangles (e) are not entangled with one another. Hence, application of Hadamard test at sites marked with blue loops, corresponding to a single sublattice, can be repeated (with reset of qubits between consecutive trials) as many times as required to achieve success.

Specifically, the repetition overhead mitigation strategy consists of applying the Hadamard test with $\mathcal{U} = e^{-i\pi\mathcal{S}}$, as in the probabilistic method described above, but only to the $\frac{N}{2}$ sites of one sublattice (cf. Fig. 4(d,e)), assuming the lattice in question is bipartite. Some of these local Hadamard tests will result in a successful symmetrization of the corresponding site (those for which the ancilla is measured in $|1\rangle$) while others will fail (those for which the ancilla is measured in $|0\rangle$). In the latter, we simply reset the qubits, reprepare the valence bonds that emanate from the respective site and try the Hadamard test again, repeating this as many times as required to obtain a successful outcome. This trial-and-error approach is only viable because next-nearest-neighboring sites are not entangled to one another in the input state, so it is possible to reset all qubits within each $4S$-qubit island (cf. Fig. 4(d,e)) without affecting the remaining qubits.

The cumulative probability of symmetrizing $\frac{N}{2}$ sublattice sites after n Hadamard test rounds is

$$P_n = (pR_n)^{N/2}, \tag{8}$$

where R_n follows the recursive relation

$$R_n = 1 + (1-p)R_{n-1},\ R_1 = 1. \tag{9}$$

As expected, R_n converges to $\frac{1}{p}$ as $n \to \infty$ so that the cumulative probability P_n approaches 1 in that limit. The average number of rounds required to symmetrize all $\frac{N}{2}$ sites of one sublattice can be computed numerically, yielding the following scaling with respect to the system size N:

$$\langle n \rangle = 1.41 \ln N + 0.484 \text{ (3 s.f.)}. \tag{10}$$

Since the circuit depth of a single layer of Hadamard tests (cf. Fig. 4(c)) is independent of N, this strategy to reduce the repetition overhead translates into an additional circuit layer of $\mathcal{O}(\ln N)$ depth. Once this step is complete, one is left with the symmetrization of only half of the sites (those belonging to the other sublattice), which requires, on average, only the square root of the original repetitions. For concreteness, for the spin-$\frac{3}{2}$ VBS on a honeycomb lattice with $N = 40$ sites, the unmitigated probabilistic method requires an average of $2^{40} \approx 1.1 \times 10^{12}$ repetitions, while the repetition overhead mitigation strategy reduces this overhead to $2^{20} \approx 1.05 \times 10^{6}$ trials.

The only element of this scheme to prepare a VBS on quantum computers for which a quantum circuit needs to be derived depending on the local spin S of the parent AKLT model is the controlled-$e^{-i\pi\mathcal{S}}$, which is, in general, a $(2S+1)$-qubit gate. For the physically relevant cases of $S = 1, \frac{3}{2}$, Mr. Murta and Prof. Fernández-Rossier performed the basis gate decomposition of the corresponding 3-qubit and 4-qubit controlled-$e^{-i\pi\mathcal{S}}$ operation [37], resulting in circuits of depth 7 CNOTs and 68 CNOTs, respectively. The prospect of faithfully implementing a circuit of such depth on near-term quantum hardware is clearly realistic.

Other Activities

In the Gutzwiller wave function project, the results were disseminated through the publication of a Letter in *Physical Review B* [3] and two conference talks, one at Session L32 (Noisy Intermediate-Scale Quantum Computers III) of the 2021 APS March Meeting and another at Session 4 (Strongly-Correlated Electron Systems) of the 3$^{\text{rd}}$ Condensed Matter Physics National Conference. In addition to the obtained results, Mr. Murta also developed valuable skills within the context of this project, including learning how to prepare mean-field states on quantum hardware through a QR decomposition via Givens rotations of the unitary transformation between the real-space basis and the tight-binding eigenbasis [5], implementing a self-consistent mean-field calculation of the Fermi-Hubbard model on conventional hardware, and adapting an exact diagonalization program based on the QuSpin package [38] to compute the Gutzwiller wave function.

Regarding the Valence Bond State project, a manuscript is currently in preparation. Although the Hadamard test used in the main method was ultimately also applied to the repetition overhead mitigation strategy, Mr. Murta and Prof. Fernández Rossier originally explored the quantum amplitude amplification algorithm [39, 40] for this purpose. In addition to becoming versed in its standard version, Mr. Murta also studied the fixed-point phase-$\frac{\pi}{3}$ method [4], since the standard approach failed to work locally for the spin-1 and spin-$\frac{3}{2}$ Valence Bond States. This project has also allowed Mr. Murta to become acquainted with the AKLT model [2] and to be introduced to the literature on measurement-based quantum computation [31, 32, 33].

Besides the study carried out within the context of the research projects, Mr. Murta has also been part of a study group dedicated to completing an online lecture course [7] on tensor network methods [6] by Prof. Jan von Delft at Ludwig-Maximilians University (Munich, Germany). Becoming instructed in tensor networks should be a useful skill not only to perform simulations of quantum many-body systems on conventional hardware but also to explore the connections between tensor network methods and quantum computing. On a final note, Mr. Murta has also delivered a tutorial on the Kitaev honeycomb model [8] at the internal meetings of the research group of which he is part. This was an opportunity to become familiar with this particular model, as well as with related concepts, notably quantum spin liquids [41] and the toric code [42].

References

[1] M. C. Gutzwiller *Phys. Rev. Lett.*, vol. 10, pp. 159–162, 1963.

[2] I. Affleck, T. Kennedy, E. H. Lieb, and H. Tasaki *Phys. Rev. Lett.*, vol. 59, pp. 799–802, 1987.

[3] B. Murta and J. Fernández-Rossier *Phys. Rev. B*, vol. 103, p. L241113, 2021.

[4] L. K. Grover *Phys. Rev. Lett.*, vol. 95, p. 150501, 2005.

[5] I. D. Kivlichan *et al. Phys. Rev. Lett.*, vol. 120, p. 110501, 2018.

[6] R. Orús *Ann. Phys. (N. Y.)*, vol. 349, p. 117, 2014.

[7] J. von Delft, "Tensor networks 2020." `https://www2.physik.uni-muenchen.de/lehre/vorlesungen/sose_20/tensor_networks_20/`, last checked on February 10, 2022.

[8] A. Kitaev *Ann. Phys.*, vol. 321, no. 1, pp. 2–111, 2006.

[9] P. W. Anderson *Science*, vol. 177, no. 4047, pp. 393–396, 1972.

[10] P. Hohenberg and W. Kohn *Phys. Rev.*, vol. 136, pp. B864–B871, 1964.

[11] W. Kohn and L. J. Sham *Phys. Rev.*, vol. 140, pp. A1133–A1138, 1965.

[12] M. Lewin, E. Lieb, and R. Seiringer *Pure Appl. Analysis*, vol. 2, p. 35, 2020.

[13] W. M. C. Foulkes *et al. Rev. Mod. Phys.*, vol. 73, pp. 33–83, 2001.

[14] M. Troyer and U.-J. Wiese *Phys. Rev. Lett.*, vol. 94, p. 170201, 2005.

[15] M. Nielsen and I. L. Chuang, *Quantum Computation and Quantum Information: 10th Anniversary Edition*. Cambridge University Press, 2010.

[16] R. P. Feynman *Int. J. Theor. Phys.*, vol. 21, no. 6, pp. 467–488, 1982.

[17] A. Y. Kitaev *arXiv:quant-ph/9511026*, 1995.

[18] A. Peruzzo *et al. Nat. Commun.*, vol. 5, no. 1, p. 4213, 2014.

[19] J. Kempe *et al. arXiv:quant-ph/0406180*, 2004.

[20] Y. Ge, J. Tura, and J. I. Cirac *J. Math. Phys.*, vol. 60, no. 2, p. 022202, 2019.

[21] S. McArdle *et al. Rev. Mod. Phys.*, vol. 92, p. 015003, 2020.

[22] P. W. Anderson *Phys. Rev. Lett.*, vol. 18, pp. 1049–1051, 1967.

[23] A. Aspuru-Guzik *et al. Science*, vol. 309, no. 5741, pp. 1704–1707, 2005.

[24] J. R. McClean *et al. Nat. Commun.*, vol. 9, no. 1, p. 4812, 2018.

[25] W. Metzner and D. Vollhardt *Phys. Rev. Lett.*, vol. 59, pp. 121–124, 1987.

[26] F. Gebhard and D. Vollhardt *Phys. Rev. Lett.*, vol. 59, pp. 1472–1475, 1987.

[27] M. C. Gutzwiller *Phys. Rev.*, vol. 137, pp. A1726–A1735, 1965.

[28] H. Tasaki, *Physics and Mathematics of Quantum Many-Body Systems*. Springer, 2020.

[29] T.-C. Wei, I. Affleck, and R. Raussendorf *Phys. Rev. Lett.*, vol. 106, p. 070501, 2011.

[30] A. Miyake *Ann. Phys.*, vol. 326, no. 7, pp. 1656–1671, 2011.

[31] R. Raussendorf and H. J. Briegel *Phys. Rev. Lett.*, vol. 86, pp. 5188–5191, 2001.

[32] R. Raussendorf, D. E. Browne, and H. J. Briegel *Phys. Rev. A*, vol. 68, p. 022312, 2003.

[33] H. J. Briegel *et al. Nat. Phys.*, vol. 5, no. 1, pp. 19–26, 2009.

[34] N. Pomata and T.-C. Wei *Phys. Rev. Lett.*, vol. 124, p. 177203, 2020.

[35] M. Lemm, A. W. Sandvik, and L. Wang *Phys. Rev. Lett.*, vol. 124, p. 177204, 2020.

[36] S. Mishra, G. Catarina, *et al. Nature*, vol. 598, no. 7880, pp. 287–292, 2021.

[37] B. Murta and J. Fernández-Rossier *In preparation.*

[38] P. Weinberg and M. Bukov, "QuSpin: a Python package for dynamics and exact diagonalization of quantum many-body systems." `https://weinbe58.github.io/QuSpin/`, last checked on February 10, 2022.

[39] L. K. Grover *Phys. Rev. Lett.*, vol. 79, pp. 325–328, 1997.

[40] G. Brassard, P. Hoyer, M. Mosca, and A. Tapp *arXiv:quant-ph/0005055*, 2000.

[41] C. Broholm *et al. Science*, vol. 367, no. 6475, p. eaay0668, 2020.

[42] A. Kitaev *Ann. Phys.*, vol. 303, no. 1, pp. 2–30, 2003.